Conference Paper, Published Version

Sakai, Hirotaka; Maeda, Kenichi

Seepage and Erosion Mechanisms of Sandy Ground Due to Air Bubbles

SEEPAGE AND EROSION MECHANISMS OF OF SANDY GROUND DUE TO AIR BUBBLES

Hirotaka SAKAI[1] and Kenichi MAEDA[2]

[1]Member of JGS, Dept. of Civil Eng., Nagoya Institute of Technology
(Gokiso-cho, Showa-ku, Naoya 466-8555, Japan)
E-mail: cgt18503@stn.nitech.ac.jp
[2]Member of ISSMGE, Associate Professor , Dept. of Civil Eng., Nagoya Institute of Technology
(Gokiso-cho, Showa-ku, Naoya 466-8555, Japan)
E-mail: maeda.kenichi@nitech.ac.jp

Seepage failure of soil and/or ground causes important geotechnical problems such as damage of dyke under flood , erosion of soil structure and ground nearby ocean and river and so on. Moreover, generation of gas and blow-out of air bubbles have been seen before seepage failure occurred in many cases. The sources of air bubbles could be thought to be air phase entrapped by seepage front and oversaturated air in pore water. The generation and the development of air bubble, therefore, play a very important role on seepage failure in nature. The air bubbles must, therefore, increase the risk of soil failure and erosion. In this paper, we focused the evolution effect of air bubbles in pore water on seepage failure. We performed model test, and developed a new numerical simulation method accounting for flowage deformation and solid-water-air bubbles interactions by Smoothed Particle Hydrodynamics. And simulation results were verified by comparison with model test results.

Key Words : *seepage failure, air bubble, three phase coupling, PIV, SPH*

1. INTRODUCTION

Large flowage deformations and hydraulic collapse of ground 'piping' which induces erosion are induced by permeation of water through ground. That plays important roles in the destabilization of ground during floods, liquefaction, erosion and so on. It is necessary to model progressive seepage failure in the soil to analyze these phenomena more precisely. Some Reports have found important roles for interactions among all three phases in solids, liquids and gases. In particular, Kodaka and Asaoka's paper[1)] might be the first article which revealed importance of dynamics of air bubbles in geoengineering. Indeed, when the Tokai flood disaster attacked Nagoya region on 11th Sept. 2000, a man saw the process of dike failure. He mentioned in a newspaper that after a crack generated on the surface of the dike, white bubbles water blew out from the dike and then dike gradually failed for about three hours. This kind of phenomena has been seen many times since old time. This blowing air bubbles before seepage failure was called 'frog blows bubbles' by elderly people. The hydraulic failure without air bubbles was defined and discussed by Terzaghi[2)].

In this study, we conducted model test and developed a new numerical simulation method for the seepage failure with air bubbles. Discrete analysis (e.g. DEM) is adapted to abruption, failure and flowage, but unsuitable procedure to analysis domain of large scale. Continuum analysis (e.g. conventional FEM) has opposite properties to that. The *smoothed particle hydrodynamics method* (SPH)[3), 4)], a completely mesh-free technique, was used to obtain the combined benefits of both distinct and continuum methods. In this study [5)-7)], SPH with a new method for calculating density, surface tension and multi-phases coupling was proposed. In this paper, the simulation results, moreover, were verified by comparison with model test results including velocity of ground and pore water pressure at failure.

2. MODEL TEST WITH IMAGE ANALYSIS

(1) Model test procedure

In model tests, we observed the deformation-failure around sheet-pile in sand ground submerged by two kind of water; one was water with low DO (demand oxygen), and another was water with high DO and over-saturated air; referred to Fig.1. In the latter, air bubble was easy to generate.

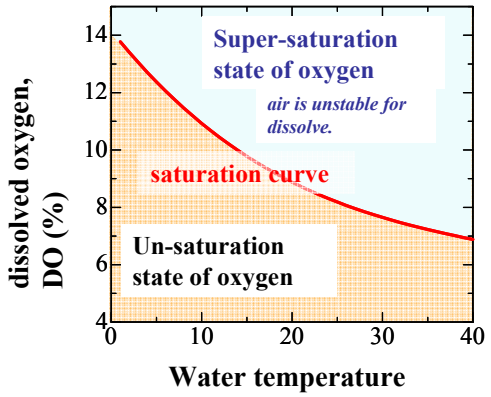

Fig. 1 *DO* (dissolved oxygen) saturation curve.

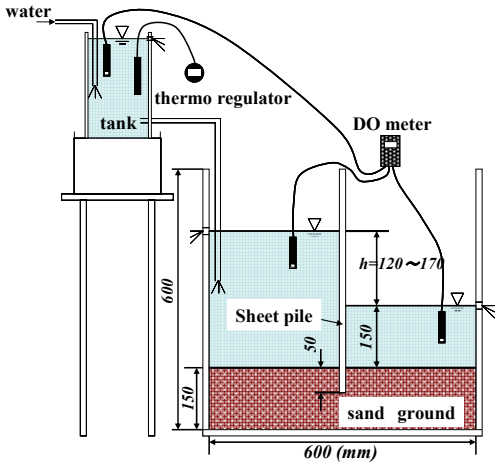

Fig. 2 Model test apparatus for seepage failure.

Two types of tests were conducted; one was 'normal piping' test with lower DO and another was 'holding' test. In the former test, a difference in water level h which was head loss applied to ground was increased to a critical head loss h_{cr} in which piping occurred in a ground; h increased within 1-2 hours gradually with a set of small increment of h and 5 minute holding. In the later test, head loss h applied was held until piping occurred. If piping did not occur even through much elapsed time passed, h was increased again to generate piping. We can measure the velocity field of ground using PIV (Particle Image Velocimetry) image analysis and calculate the strain rate fields from image analysis results. We follow the test apparatus shown in Fig.2 and test condition as experiments performed by Kodaka and Asaoka[1]. Toyoura sand was employed. The dissolved oxygen (*DO*), water temperature, and permeable water volume of the ground were measured. A tensiometer pressure sensor was equipped at the 50mm right horizontally from the tip of the sheet-pile in the down-stream.

(2) Model test results and discussions

Fig.3 and Fig.4 show the typical deformation-failure behaviours around sheet-pile for lower *DO* and higher *DO* cases, respectively. Fig. 5 shows the relative applied head loss h/h_{cr} indicating safety against piping with elapsed time after h was increased and/or held. In the case of lower *DO* in the normal piping test, piping occurred at h/h_{cr} =1 according to the definition. However, in the case of higher *DO*, even though h is than h_{cr}, air bubbles were generated as shown in Fig. 4, and consequently, failure occurred in holding test. When the water level was increased after holding the smaller water level difference h for a long time, the failure tended to occur even before the water level difference reached the critical level h_{cr}: $h/h_{cr} < 1$; it is similar to creep failure in a material under constant load smaller than the strength. This implies that air bubbles in ground bring strength degradation. The relationship between the air bubble generation and *DO* and the influence of air bubbles on the ground were investigated in the following sections.

(upstream) (downstream)

Fig. 3 Piping with water of lower *DO* and without air bubbles in normal piping test: increasing head loss h to h_{cr}.

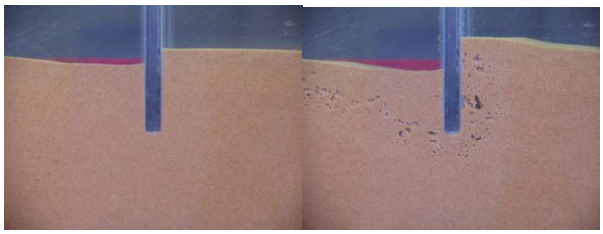

(start of holding test) (elapsed time after holding: 94hr)

Fig. 4 Deformed ground just before piping with water of higher *DO* in holding test: holding head loss $h = 0.8 \times h_{cr}$.

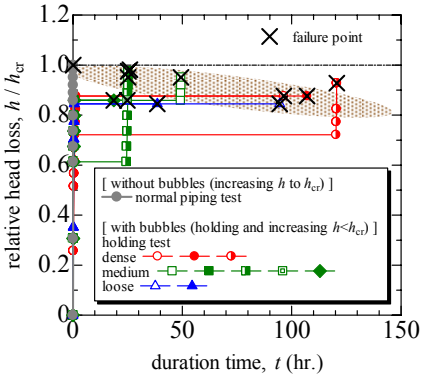

Fig. 5 Decrease in safety against piping due to air bubbles.

In seepage failure without air bubbles as shown in Fig.6, ground subsidence (scour) at the upstream side and ground uplift (roll-up) at the downstream side occur continuously when $h/h_{cr} > 0.90$. However, in the case with air bubbles as shown in Fig.7, the ground surface at the downstream side was displaced intermittently. This must be related to the dynamics of air bubble such as the generation and development, movement, and ejection of air bubbles from the ground. Fig.8 shows both of change in amount of air bubbles at the downstream side which was calculated by image analysis and change in void ratio estimated by assuming that void changed due to only air bubbles. Here, the rapid descend points mean the bubble ejection with rapid subsidence of ground. Moreover, since the accumulated amount of air bubbles was limited as shown in Fig.8, the ground surface at the downstream side was not displaced for a while following the ejection of large air bubbles. On the other hand, the ground surface at the upstream side was not displaced for a while, but it was suddenly displaced after a period of time; we can observe this visually in Fig.9. Consequently, the displacement in the ground at the downstream side gradually propagated to the ground at the upstream side, passing below the sheet pile, accompanied by the intermittent ejections of air bubbles accumulated in the ground at the downstream side. This resulted in the ground surface subsidence at the upstream side.

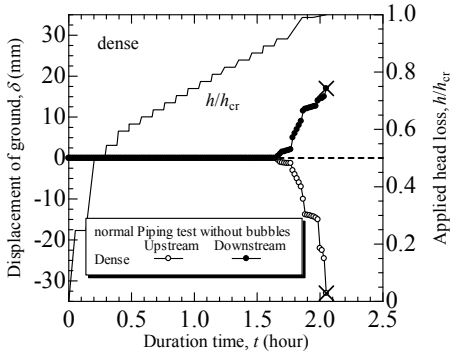

Fig. 6 Displacement of ground surfaces in upstream and down stream for normal piping test without air bubbles due to application head loss.

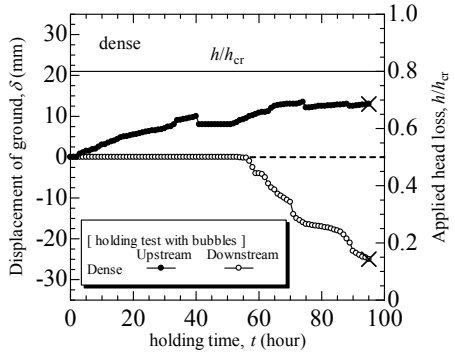

Fig. 7 Displacement of ground surfaces in upstream and down stream for holding test with air bubbles due to application head loss.

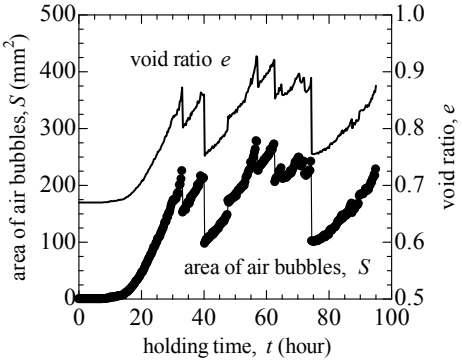

Fig. 8 Changes in amount of air bubbles in downstream around sheet-pile and in void ratio calculated according to Fig.7.

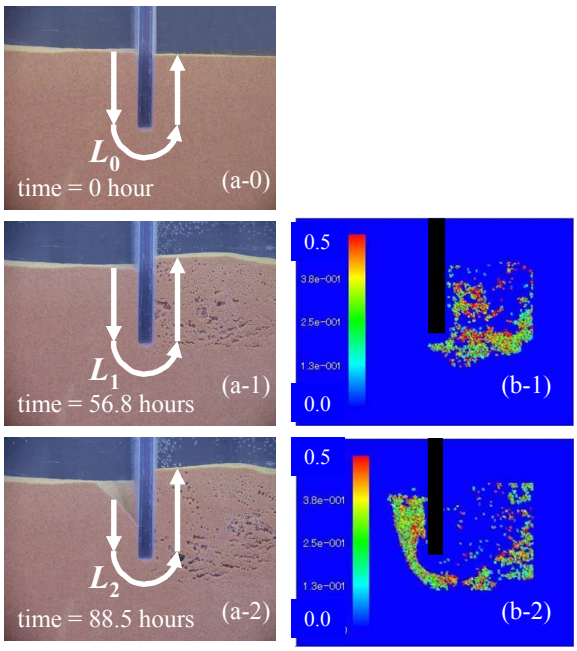

Fig. 9 Variations of length of seepage around sheet-pile and maximum shear strain rate distribution, referred to Fig.7.

Those dynamics of air bubbles bring frequent change in void ratio. Since the critical hydraulic gradient i_{cr} of ground is calculated by $i_{cr} = (G_s\text{-}1) / (1+e)$ where G_s is soil particle specific weight [2], as shown in Fig. 10. From the photographs, seepage distances L around sheet-pile can be calculated. Before ground subsidence at the upstream occurs, L becomes longer;

$L_0 < L_1$. And then L becomes shorter; $L_2 < L_1$. Consequently, the hydraulic gradient i increases, expressed in Fig.10, even through head loss h is constant. Normally, ordinate seepage failure occurs when the seepage force increases due to an increase in head loss. However, even though the head loss was held, the residence against piping i_{cr} decreased and seepage load i increased due to the abovementioned mechanism, and consequently, seepage failure occurred.

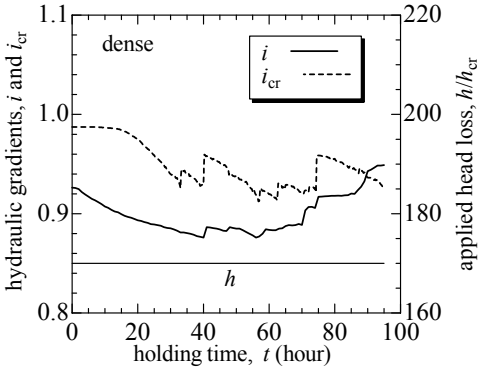

Fig. 10 Changes in hydraulic gradients due to generation of air bubbles and deformation of ground evolution of air bubbles even with constant head loss, according to Fig.7.

3. NUMERICAL ANALYSIS: SPH

(1) Analysis procedure

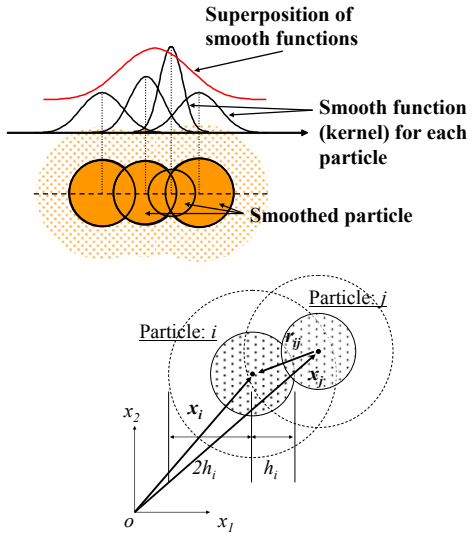

Fig. 11 Particle and smoothing function in SPH.

SPH is a particle-based Lagrangian method. This method was originally developed by Gingold & Monaghan[3] and Lucy[4] in astrophysics to solve motions of galaxies. Then, this method was applied to viscid flows and failure of solids. The SPH is intended not for treating the actual soil grain but for solving "particle" as soil mass (Fig. 11), whose radius is h. Similarly water "particle" is a finite volume of water but not a molecule. These particles can overlap. Since this method is Lagrangian, it can also express sliding, contact, separation, and two or three phase interactions. The spatial averaged value $<f(\mathbf{x})>$ of physical quantity $f(\mathbf{x})$ at point x is given by Eq. (1). Particles $\mathbf{x}'$ with $f(\mathbf{x}')$ are located within the zone of influence of the first particle ($2h$). The physical quantity is interpolated using a smoothing function W (see Figs. 11).

$$f_i = < f(\mathbf{x}_i) > \cong \sum_{j=1}^{N} m_j \frac{f_j}{\rho_j} W_{ij}(\mathbf{r}_{ij}, h) \tag{1}$$

where $\mathbf{r} = \mathbf{x}_i - \mathbf{x}_j$ and W is defined by,

$$1 = \int W(\mathbf{r}, h) d\mathbf{x}' \tag{2}$$

In this paper, 3rd B-spline function was employed as W, and $r_{ij} = |\mathbf{r}_{ij}|$ and $S = r_{ij}/h$ are used,

$$W_{ij} = \frac{15}{7\pi h^2} \times \begin{cases} \frac{2}{3} - S^2 + \frac{1}{2}S^3 & 0 \le S < 1 \\ \frac{1}{6}(2-S)^3 & 1 \le S \le 2 \\ 0 & 2 < S \end{cases} \tag{3}$$

The density ρ_i of particle i is replaced with f_i ,

$$\rho_i = \sum_{j=1}^{N} m_j \frac{\rho_i}{\rho_j} W_{ij} = \sum_{j=1}^{N} m_j W_{ij} \tag{4}$$

However, this description shows large error in densities calculated by original theory around the interface. We improved this point by normalization and limited summation for a material focused (e.g. *material a*)

$$\rho_{i \in Material\ a} = \frac{\sum_{j=1 \in Material\ a}^{N} m_j W_{ij}}{\sum_{j=1 \in Material\ a}^{N} \left(\frac{m_j}{\rho_j} \right) W_{ij}} \quad \text{for } material\ a; \tag{5}$$

The SPH description for particle i in motion equation can be explained as follows.

$$\frac{d\mathbf{v}_i}{dt} = -\sum_{j=1}^{N} m_j \left(\frac{\boldsymbol{\sigma}_j}{\rho_j^2} + \frac{\boldsymbol{\sigma}_i}{\rho_i^2} + \Pi_{ij}\mathbf{I} \right) \cdot \nabla W_{ij} + \mathbf{f}_i \tag{6}$$

where $\boldsymbol{\sigma}$ and $\mathbf{f}$ are stress tensor and body force, respectively. The matrix $\mathbf{I}$ is unit matrix, and Π_{ij} is the artificial viscosity.

For the purpose of coupling, the soil and the fluids

of water and air were handled on different layers (see Fig. 12). The frictional body forces resulting from velocity differences between two phases, v^s and v^f were employed with the Biot's mixture theory[8]. The forces can be expressed as follows:

$$\mathbf{f}^{sf} = n\frac{\rho_f g}{k}\left(\mathbf{v}^s - \mathbf{v}^f\right), \quad \mathbf{f}^{fs} = n\frac{\rho_f g}{k}\left(\mathbf{v}^f - \mathbf{v}^s\right) \qquad (7)$$

Here, porosity n, permeability k, fluid density ρ_f and gravity acceleration g are included.

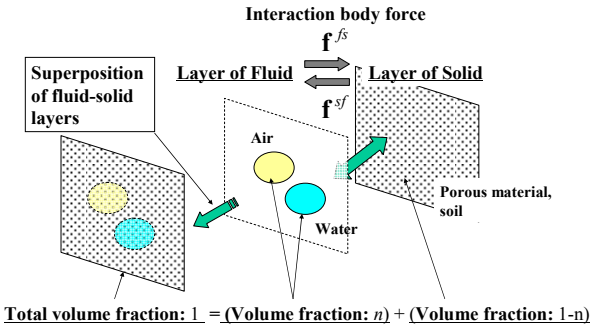

Fig. 12 Interaction force to coupling between solid-liquid-gas.

The boundary was reproduced by creating an array of virtual boundary particles. The leap-frog method with time step was used holding the CFL conditions.

(2) Analysis results and discussions

Figures 13 and 14 show the results of the analyses for the collapse of columns of water and frictional material, respectively. The final surface of water column broken becomes flat, but the surface in Fig.14 is inclined. These tendencies agree with actual flows.

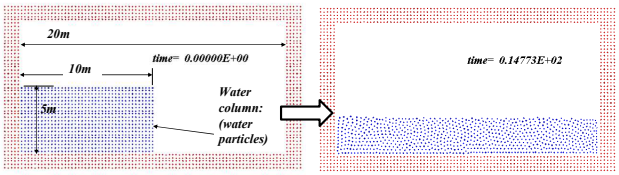

Fig. 13 Collapse analysis of water column (dam break).

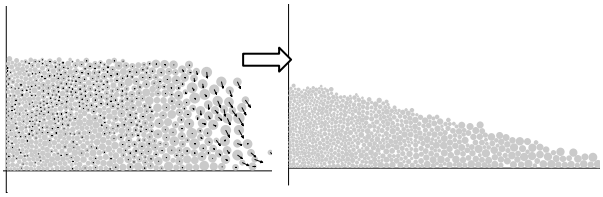

Fig. 14 Collapse analysis of frictional material column.

Figure 15 shows analysis result of the rise process of air bubbles in water. The bubbles were simulated using clusters of SPH gas particles. We involved surface tension effect by adding force term.

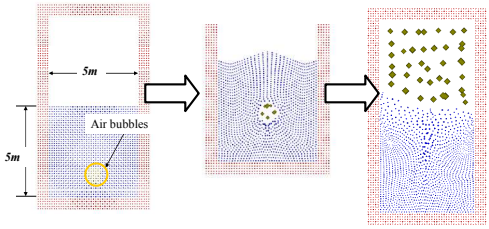

Fig. 15 Analysis of bubbles in water.

Figure 16 shows an SPH model of the experiment shown in Fig. 3 without air bubbles. This model can simulate characteristics of seepage failure well not only during deformation but also after the failure.

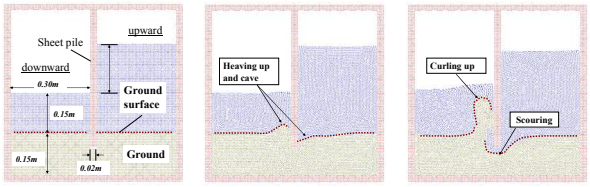

Fig. 16 Seepage failure analysis around sheet pile without air bubbles; generation of failure of ground when $h=h_{cr}$.

We can see not only the concentration of flow around the tip of the sheet-pile but also the existence of high speed in the downstream side due to curling induced by the erosion. Fig.17 and Fig.18 show comparisions between model test results and numerical simulation results for velocity field and for pore water pressure in the ground around the sheet-pile at piping failure. The velocity of ground measured by PIV is shown in Fig.17(a) and the velocity at the 50mm right horizontally from the sheet-pile tip in the down-stream after the failure is about 0.3m/s, which might be same as the velocity of water in mixed. The SPH simulation result for velocity at the tip of the sheet pile in Fig.17(b) is 0.28m/s, and this is almost same as that of the model test. The pore water pressure at the same point measured by the tensiometer is shown in Fig.18(a) and the value at the failure state is around 2500Pa. And the pressure distributions around the above are of ground in the down-stream are influenced by the curling flow due to the erosion. The pressure value analyzed in the down-stream around the tip in Fig.18(b) is almost same as that of model test. The analysis results show good agreement with model test results. The analysis show good performance qualitatively and quantitatively.

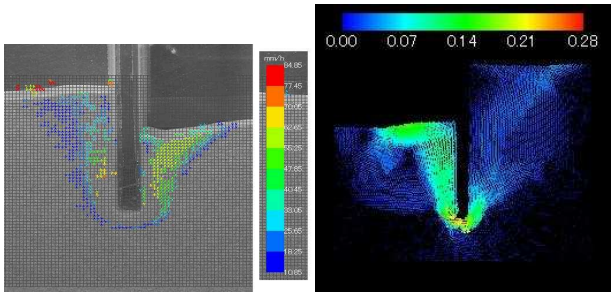

(a) model test (unit: *mm*/*hr*) (b) simulation (unit: *m*/s)

Fig. 17 Comparison in velocity distributions around sheet-pile without air bubbles; PIV image of ground velocity for model test; (b) water velocity for SPH simulation.

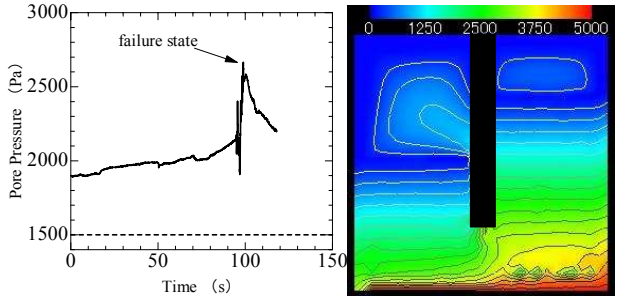

(unit: Pa)

(a) model test (b) simulation

Fig. 18 Comparison in pore water pressure around sheet-pile without air bubbles at piping; (a) from tensiometer pressure sensor in model test; (b) from SPH simulation.

Fig. 19 shows a SPH prediction of seepage failure around sheet pile with air bubbles under 80% of water height difference in Fig.16. In this analysis, air phase was replaced forcedly with another phases at initial state; the generation of air bubbles will be able to be involved concerning entropy and enthalpy in the future work. The failure of ground is induced by air bubbles rise as same as experiments. We can find that the movement of air bubbles induces the local deformation of the ground.

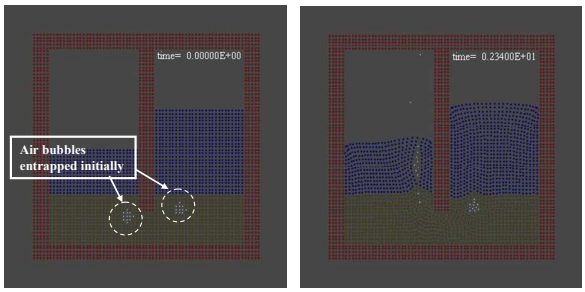

Fig. 19 Seepage failure analysis with air bubbles; generation of local failure occurs at local even when h=0.8 × h_{cr}.

4. CONCLUSIONS

From model test results by using PIV image analysis, it was revealed that the dynamics of air bubbles in the ground caused the degradation of the ground. Even though the head loss was held to be constant value less than critical head loss, the residence against piping i_{cr} decreased and seepage load i increased. In next stage, we will reveal the interaction detail mechanism between the degradation of the ground and the evolution of air bubbles.

This paper proposed a newly developed method of SPH to solve three-phase systems (solid, liquid and gas). This paper showed clearly the validation and usefulness of SPH to be applicable for problems three phase. The analysis performance is qualitatively high. Some analysis results were verified with model test results and we found the accuracy of this proposed analysis procedure although we conducted the verification in only some data. The procedure will be able to be developed to simulate seepage failure from the generation of the bubbles to the evolution.

ACKNOWLEDGMENT: The authors are grateful to the Japan Society for the Promotion of Science for its financial support with Grants-in-Aid-for Scientific Research (B) 20360210.

REFERENCES

1) Kodaka, T. and Asaoka, A.: Formation of air bubbles in sandy soil during seepage process, *Journal of JSCE*, Vol. 487 (III-26), pp.129-138 (in Japanese), 1994.
2) Terzaghi, T.: *Theoretical soil mechanics*, john Wiler and Sons, INC., 1942.
3) Gingold, R.A. and Monaghan, J.J.: Smoothed particle hydrodynamics: theory and application to non-spherical stars, *Monthly Notices of the Royal Astronomical Society*, Vol.181, pp.375-389, 1977.
4) Lucy, L. B.: A numerical approach to the testing of the fission hypothesis, *Astronomical Journal*, Vol.82, pp.1013-1024, 1977.
5) Maeda, K. and Sakai, M.: Development of seepage failure analysis procedure of granular ground with Smoothed Particle Hydrodynamics (SPH) method, *Journal of Applied Mechanics, JSCE,* Vol.7, pp.775-786. (in Japanese), 2004.
6) Maeda, K., Sakai, H. and Sakai, M.: Development of seepage failure analysis method of ground with smoothed particle hydrodynamics, *Jour. of Structural and earth-quake engineering, JSCE, Division A*, Vol.23, No.2, pp.307-319, 2006.
7) Sakai, H. and Maeda, K.: A study on seepage failure of sand ground with account for generation and development of air bubbles, *Proc. of 13th Asian Regional Conference on Soil Mechanics and Geotechnical Engineering*, pp.571-574, 2007.
8) Biot, M. A.: General theory of three dimensional consolidation, *Journal of Applied Physics*, Vol.12, 152-164, 1941.